An investigation into the effect of input function shape and image acquisition interval on estimates of washin for dynamic cardiac SPECT

Steven G Ross†, Andy Welch†§, Grant T Gullberg†‖ and
Ronald H Huesman‡

† University of Utah, Salt Lake City, UT, USA
‡ Lawrence Berkeley National Laboratory, University of California, Berkeley, CA, USA

Abstract. Dynamic cardiac SPECT and PET can be used to measure myocardial perfusion by estimating the kinetic rate constant describing the washin of radioactive-labelled tracers from the blood to the extravascular myocardial tissue. Because of differences in photon statistics and data acquisition techniques, protocols which produce optimal estimates of the washin for dynamic cardiac PET may give suboptimal estimates if applied in dynamic cardiac SPECT. Two important factors in the estimation of washin are the shape of the tracer input function and the image acquisition interval. This study uses computer simulations to investigate the effect of varying the tracer infusion length and image acquisition interval on the bias and variance of estimates of washin obtained with dynamic cardiac SPECT and ^{99m}Tc-labelled teboroxime. Bias in parameter estimates can be introduced by aliasing, integration of the time-varying radioactivity by the detector, and detector motion. This bias can be reduced by decreasing the acquisition interval and using a longer-duration input function. However, this results in poor photon statistics, which generate large variance, and can also introduce bias in the estimates of the washin. Our studies indicate that better estimates of the washin are obtained by using an acquisition interval that is of sufficient duration to obtain adequate photon statistics even if this is at the expense of temporal resolution. The increase in bias caused by using a 10 or 20 s acquisition interval instead of a 5 s acquisition interval is minimal when compared with the reduction in variance. Variance in estimates is also reduced by using a sharp input function, resulting in higher peak counts during washin. It is also shown that the variance of estimates of the washin increases generally when faster kinetics are observed. This variance can, however, be reduced by using longer acquisition intervals.

1. Introduction

Single-photon emission computed tomography (SPECT) is used to infer variation in cardiac perfusion through visual interpretation of static images. It is possible, however, to obtain measurements of myocardial perfusion by tracking the kinetics of the radioactive-labelled tracer as it passes through the heart. Measures of myocardial perfusion are obtained by using dynamic imaging to estimate the kinetic parameters describing the exchange of radioactive-labelled kinetic tracers between the blood and the myocardial tissue. Estimates of these kinetic parameters are correlated to perfusion and may give more sensitive measurements

§ Andy Welch is presently at the University of Aberdeen, Scotland.
‖ Please send correspondence to Grant T Gullberg, PhD, Department of Radiology, Medical Imaging Research Laboratory, AC-213 Medical Center, University of Utah, Salt Lake City, UT 84132, USA.

of ischaemia than visual interpretation of static images. Dynamic positron emission tomography (PET) has been shown to be effective for estimating kinetic rate constants (Muzik *et al* 1993, Herrero *et al* 1992, Bergmann *et al* 1989, Mullani *et al* 1983), while dynamic SPECT also can be used to estimate kinetic parameters (Smith and Gullberg 1994, Smith *et al* 1994, 1996). Dynamic SPECT does, however, suffer from certain disadvantages when compared to dynamic PET. These include poor resolution (Welch *et al* 1995), large effects from photon attenuation (Gullberg *et al* 1985, Smith and Gullberg 1994), and increased blurring from geometric point response (Zeng *et al* 1991, Zeng and Gullberg 1992). All of the aforementioned effects can introduce bias into estimates of myocardial perfusion.

Another major drawback to dynamic cardiac SPECT is poor photon statistics which introduce large variances into the estimates. SPECT has poorer photon statistics than PET in large part because of the need for detector collimation, which severely decreases the number of detected photons. Photon statistics are further degraded in dynamic SPECT because of the need to acquire sufficient temporal information to adequately track the time-varying dynamics of the radioactive labelled tracer. In a typical static SPECT scan, projection data are obtained over 360° in approximately 20–30 min. In order to track the time-varying tracer, dynamic SPECT usually requires acquisition of 360° projection data in approximately 5–40 s, over a total duration of 10–15 min. This results in much poorer photon statistics in each dynamic projection set.

The poor photon statistics associated with these short acquisition intervals are evident from ongoing canine studies being carried out by this research group. In these studies, a three-detector SPECT system is used to track these dynamic changes. To do this, the camera gantry is rotated at high rates with the maximum rotation rate giving 360° of coverage in 5 s. Five second acquisitions are then acquired for a duration of 15 min after the injection of teboroxime. In a dog weighing approximately 35 kg, a bolus injection of 15 mCi ^{99m}Tc-labelled teboroxime yields approximately 320 000 counts in the maximum 5 s projection set ($64 \times 64 \times 60$ angles). Welch *et al* (1995) demonstrated that kinetic parameter estimates are severely degraded when count levels approach these low ranges. It was shown, however, that slight improvements in count levels, e.g., from 320 000 counts in the maximum projection set (5 s acquisition intervals) to 640 000 counts, result in significant reduction in the variance of the kinetic parameter estimates.

Photon statistics can be improved by increasing the dose of ^{99m}Tc-labelled teboroxime. However, there are limits on photon counts set by injection levels of the radioactive-labelled tracer, the counting rates of the camera, and other count-limiting factors such as body attenuation. Once count rates have been maximized within these limits, count rates can be further improved by increasing the image acquisition interval (slowing the detector gantry). Another and perhaps more optimal approach would be to increase count rates by summing projection data from several acquisitions.

Increasing the acquisition interval by slowing the detector gantry adversely affects temporal resolution by not adequately sampling the time-varying dynamics of the tracer. Aliasing arises from insufficient sampling of the time-varying tracer. To reduce aliasing the acquisition interval can be decreased, resulting in better sampling, or the infusion can be dispersed over time, resulting in a smoother time-varying activity with less high-frequency content. The disadvantage of both of these techniques is that they result in fewer peak counts in the dynamic projection sets, which in turn results in less accurate kinetic parameter estimates.

Another effect which introduces bias into kinetic parameter estimates is the relative starting point of the time–activity curves with respect to the acquisition interval of the

photon detector over each dynamic sampling period. The counts in each projection bin are not an instantaneous sample of the tracer, but rather are the result of photons detected over a finite time interval. Thus, the sampled points are actually the result of integration of the tracer and each acquired sample in the detector is the integral of all counts in the acquisition period. This causes the kinetic parameter estimates to be sensitive to the time at which the tracer is injected with respect to the time at which the detector begins acquiring data.

The rotation of the gantry also affects the kinetic parameter estimates. Data inconsistencies arise because the tracer activity and the projection angle are changing as data are being acquired. Detector motion is specific to the rotating gantry systems and can be avoided by using a static ring system. Static ring detector systems are commonly utilized in dynamic PET and have been introduced in dynamic SPECT (Stewart *et al* 1990); however, their use in SPECT is not widespread due to the cost and their limited number of applications.

This paper describes a study which investigates the effect of input function infusion length and image acquisition interval on the bias and variance of estimates of the washin of ^{99m}Tc-labelled teboroxime from the blood to the myocardial tissue obtained with dynamic cardiac SPECT. There have been research efforts investigating the effect of input function shape and acquisition interval on kinetic parameter estimation in dynamic PET (Mazoyer *et al* 1986, Cunningham and Jones 1993, Herrero *et al* 1989). However, dynamic cardiac SPECT suffers from much poorer photon statistics than those observed in dynamic cardiac PET. Because of this, protocols which produce optimal estimates of washin for dynamic PET may give suboptimal estimates if applied in dynamic cardiac SPECT. Also, detector motion can introduce bias which would not be present in dynamic PET studies. Computer simulations are carried out to study the effects of input function shape and image acquisition interval on aliasing, integration, detector motion, and photon statistics.

2. Background

To track the time-varying activity of the radioactive-labelled tracer injected into the body, dynamic projection sets are acquired over a finite period of time which is sufficient to view the temporal changes of the tracer. In experiments in our laboratory, the projections are acquired from a triple-detector SPECT system in which the detector gantry can be rotated through $120°$ in as little as 5 s to provide $360°$ angular coverage. Generally, 5 or 10 s rotation rates have been employed in our investigations. Projection sets are acquired over 15 min, resulting in 90–180 dynamic projection sets, depending on the gantry rotation rate. Dynamic images are then reconstructed from these projection sets using the expectation-maximization–maximum-likelihood (EM–ML) algorithm (Shepp and Vardi 1982, Lange and Carson 1984).

Of interest is the time-varying activity in the ventricular blood pool and localized regions of the myocardial tissue. The activity in these locations is determined by drawing regions of interest (ROIs) on the reconstructed images and sampling the tracer activity in these ROIs for each dynamic image. A one-compartment model is used to relate the time–activity curves in the blood and myocardium ROIs to the exchange of tracer between the blood and myocardial tissue. This exchange between the blood concentration $B(t)$ and the tissue concentration $C(t)$ is modelled with the kinetic parameters k_{21} (washin) and k_{12} (washout) with units of millilitres per minute per millilitre of extravascular space using the following differential equation:

$$\frac{\mathrm{d}}{\mathrm{d}t}C(t) = k_{21}B(t) - k_{12}C(t) \qquad (1)$$

with solution

$$C(t) = k_{21} \int_0^t e^{-k_{12}\tau} B(t - \tau) \, dt. \tag{2}$$

Equation (2) states that the tissue concentration is a convolution of the blood activity and an exponential kernel which is a function of the rate constants. The tracer activity in the myocardium region of interest depends not only on the tissue activity, but also on the fraction of blood f_v that is present in the tissue, e.g., in the capillaries. Also, the activity cannot be sampled instantaneously, but rather is sampled over integrated time periods Δt which are equal to the image acquisition interval (the rate of rotation of the SPECT system). Taking these factors into account, the total activity $A(t)$ in the tissue ROI is written as

$$A(t) = (1 - f_v)k_{21} \int_{t-\Delta t}^t \left[\int_0^t e^{-k_{12}\tau} B(t - \tau) \, d\tau \right] dt + f_v \int_{t-\Delta t}^t B(t) \, dt. \tag{3}$$

Given blood and tissue time–activity curves, $B(t)$ and $A(t)$, as well as the acquisition interval Δt, the kinetic parameters k_{21}, k_{12}, and the blood fraction f_v are estimated with RFIT (Coxson *et al* 1992, Huesman and Mazoyer 1987, Huesman *et al* 1995). RFIT uses weighted least squares to estimate kinetic parameters from computational models with the form of equation (3) and, if necessary, for a noisy input function.

RFIT requires for input the curves $B(t)$ and $A(t)$ and the variance of $B(t)$ and $A(t)$, as well as the covariance between $B(t)$ and $A(t)$. In this paper the estimated blood and tissue variances are approximated to be equal to the ROI counts. This estimate is expected to be proportional to the error on the reconstructed count density using the EM–ML algorithm, although it does not represent the true errors in the ROI (Wilson and Tsui 1993, Barrett *et al* 1994, Wilson *et al* 1994). The tissue–blood covariances are estimated to be zero in this analysis. An incorrect estimate of the ROI variance and blood–tissue ROI covariance generally gives rise to an increase in the bias and variance associated with the kinetic parameter estimates (Gullberg *et al* 1997, Huesman and Mazoyer 1987).

Once estimates of the kinetic parameters are obtained, they can be used to obtain an estimate of flow multiplied by extraction in the myocaridal tissue. This measure can then be correlated to flow. Washin, k_{21}, has been shown to be correlated to myocardial perfusion in dynamic cardiac SPECT (Smith and Gullberg 1994, Smith *et al* 1994, 1996). The parameter k_{12} is also correlated to flow; however, this correlation is not as strong as that seen in k_{21}. Because of this, the results presented in this paper will focus only on the parameter k_{21}.

3. Methods

The clinical dynamic SPECT system to be modelled consists of three detectors which are each rotated through 120° (360° coverage) to acquire each dynamic projection set. The detector can be rotated at different speeds; consequently the acquisition interval can be varied, with a minimum 120° rotation time of 5 s. Four different acquisition intervals are studied: 5, 10, 20, and 40 s. Four tracer infusion lengths are also studied: a bolus and 30, 60, and 90 s infusions. Sections 3.1 and 3.2 analyse ideal input functions which are not obtained from tomography, while sections 3.3 and 3.4 analyse input functions obtained from reconstructed tomographic images.

3.1. Aliasing

Effects due to undersampling of the blood and tissue time–activity curves are addressed first. The time–activity curves are based on canine studies by Smith *et al* (1994) with the

tracer time–activity in the blood pool for a bolus infusion modelled as

$$B(t) = \begin{cases} 450t/20 & t \leqslant 20 \\ 400\,\mathrm{e}^{-0.1(t-20)} + 50\,\mathrm{e}^{-0.001(t-20)} & t > 20. \end{cases} \quad (4)$$

Blood time–activity curves for 30, 60, and 90 s infusions are simulated by convolving equation (4) with 30, 60, and 90 s step functions, respectively. The myocardial tissue activity is simulated with kinetic values typical of those observed in a resting dog with $f_v = 0.15$, $k_{21} = 0.8$ min^{-1}, and $k_{12} = 0.4$ min^{-1}. Kinetic rate constants typical of those observed in a dog vasodilated with adenosine were also used with $k_{21} = 4.0$ min^{-1}, $k_{12} = 2.0$ min^{-1}, and $f_v = 0.15$. The frequency spectra of the time–activity curves are determined with an analytic Fourier transform of the time–activity curves. The spectra are used to demonstrate the aliasing associated with the time–activity curves. To simulate the finite acquisition period of the photon detector, the time–activity curves are sampled every $0.031\,25$ ($\frac{1}{32}$) s and these values are integrated over finite intervals which correspond to the acquisition interval of the detector (5, 10, 20, and 40 s). The integrated data are used in RFIT to estimate the kinetic parameters k_{21}, k_{12}, and f_v.

3.2. Photon integration

Each data point that is used in the estimation of the kinetic parameters is the integral of the continuously varying time–activity curve. This integration can potentially result in a misrepresentation of the actual time–activity curve and subsequently introduce bias into kinetic parameter estimates. The misrepresentation of the signal is most severe when the integration period of the detector ends near the peak of the input function. This causes the peak of the input function to be represented by approximately equal points on either side of the peak. This misrepresentation of the signal can potentially introduce bias into kinetic parameter estimates. This causes the kinetic parameter estimates to be dependent on any time shift of the time-varying tracer with respect to the integration period of the detector, which could occur by not properly timing the injection and the starting point of the acquisition. A reduction in bias can be achieved by optimizing the starting time point of the tracer infusion with respect to the starting acquisition interval of the detector. This effect is investigated by shifting the starting point of the time–activity curves to optimize the parameter estimates. The input functions are shifted by quarter intervals of the acquisition interval to obtain optimum estimates of washin. Delay intervals of 0, 1.25, 2.5, and 3.75 s are used for 5 s acquisitions; delay intervals of 0, 2.5, 5.0, and 7.5 s are used for 10 s acquisitions; delay intervals of 0, 5, 10, and 15 s are used for 20 s acquisitions; and delay intervals of 0, 10, 20, and 30 s are used for 40 s acquisitions.

3.3. Detector motion

The next group of simulations addresses effects from tomography and detector motion. These simulations model a clinical three-detector SPECT system. The geometry is modelled with a modified version of the MCAT heart and torso phantom (Tsui *et al* 1994, Terry *et al* 1990). A single transaxial slice of the phantom is shown in figure 1. The phantom consists of three regions; myocardial tissue, blood pool, and a uniform background with 20% of the activity in the blood pool. Time-varying activity in the phantom is simulated with the time–activity curves corresponding to a bolus infusion and a 90 s infusion. The MCAT phantom is discretized into 128×128 pixels and 60 angular unattenuated fan beam projections are formed with a ray-driven, line-length weighting projector (Huesman *et al* 1977). The
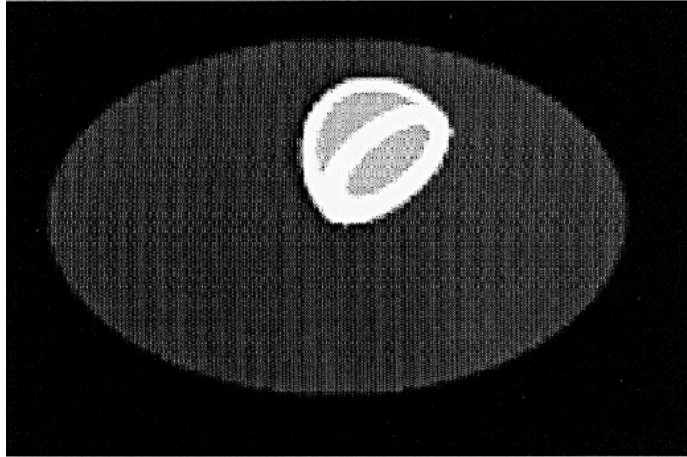
Figure 1. A transaxial slice of the MCAT phantom used in the simulations to generate the emission data.

projections are discretized into 128×2 bins which are subsequently binned to 64×1. The size of each pixel is 0.712 cm, the radius of rotation is 34 cm, and the centre of rotation is at the centre of the phantom. Because of the fan beam geometry, the projection data truncates 32% of the MCAT phantom.

Each of the 60 projections in a $360°$ tomographic set is the average of a certain number of subprojections (over six degrees). To simulate the varying image acquisition intervals ($360°$ detector rotation time), each subprojection is obtained every 0.03125 s; however, the number of subprojections per $6°$ angular bin is varied. Thus a 5 s image acquisition interval used eight subprojections per $6°$ angular bin, a 10 s interval used 16 subprojections, a 20 s interval used 32 subprojections, and a 40 s interval used 64 subprojections. The 60 projections are then used to reconstruct a 64×64 transaxial image with the expectation-maximization–maximum-likelihood algorithm (EM–ML) (Shepp and Vardi 1982, Lange and Carson 1984). The bias in the parameter estimates is observed as a function of the number of iterations of the EM–ML algorithm. The projection data are also reconstructed using filtered backprojection with a ramp filter with cutoff frequency of 0.5 cycles/projection bin. Filtered backprojection is used for comparison purposes with the EM–ML algorithm; however, it is not used when photon noise is included in the simulations. A single transaxial slice is used to draw blood and tissue ROIs. The blood ROI is 7.2 cm^3 and the tissue ROI is 4.2 cm^3.

3.4. Photon statistics

Poisson noise is added to the projection sets to simulate the statistics observed in canine studies in our laboratory. In these studies, an injection of 15 mCi ^{99m}Tc-labelled teboroxime resulted in approximately 320 000 counts in the maximum $360°$ 5 s projection set over the 10 min dynamic acquisition, while injections of 30 mCi ^{99m}Tc-labelled teboroxime resulted in approximately double these counts.

Blood and tissue time–activity curves are obtained from dynamic images reconstructed with 25 iterations of EM–ML using the moving detector system and the MCAT phantom. The projection data are generated as described in section 3.3. Poisson noise is added to each projection set with a scaling factor set to ensure that the appropriate statistics were observed for all acquisition intervals and input functions. In all cases one hundred

realizations were performed with different seeds used for the random number generator. Estimates are obtained for each realization and the results show the population mean of these estimates along with the population standard deviation. In addition, the variance in the estimates is plotted against the absolute bias.

4. Results

The results of sections 4.1 and 4.2 were calculated with integration of the exact blood and tissue time–activity curves. The results of sections 4.3 and 4.4 were calculated using simulated projection data of the MCAT phantom. In sections 4.3 and 4.4, estimates are obtained using time–activity curves obtained from ROI analysis on reconstructed transaxial slices of the MCAT phantom.

4.1. Aliasing

The blood and tissue time–activity curves are shown in figure 2(a)–(c). The Fourier transforms of these curves are shown in figure 3(a)–(c) respectively. The vertical lines correspond to the frequency that could be recovered for a given acquisition interval (5, 10, 20, or 40 s) based on Nyquist's theorem. For example, an acquisition interval of 5 s can recover frequencies below $1/(2 \times 5 \text{ s})$. The frequency spectra of figure 3(a) show that the vast majority of the blood signal is recovered with 5 s acquisition intervals. Higher frequencies of the bolus infusion are lost with 10 s acquisitions, and a significant amount of the spectrum is lost with 20 and 40 s acquisitions. As the infusion is lengthened, a much smaller portion of the frequency response is lost.

Figure 3(b) and (c) shows the frequency spectra for the tissue curves. The majority of the frequency components are recovered for 5 and 10 s acquisitions using resting parameters. There are substantial frequency components lost with 20 and 40 s acquisition intervals, particularly for the bolus and 30 s infusions. The frequency spectrum of the vasodilated tissue curve shows that a much greater portion of the signal is lost than in the resting case.

Figure 4 shows estimates of k_{21} for the resting kinetic parameters. The results are obtained by integrating the time–activity curves over the acquisition interval and using RFIT to obtain estimates of k_{21}. The plot shows that the most accurate estimates are obtained with 5 s acquisitions, with bias increasing as the acquisition interval is increased. In general, bias is maximum for a bolus infusion because the aliasing is greatest, while the least bias is seen with a 90 s infusion. There are apparent anomalous results for 20 and 40 s acquisition intervals. For instance, when a bolus infusion is simulated, the bias in washin of a 20 s acquisition is greater than that of a 40 s acquisition. Also, the bias for the 30 s infusion is disproportionately large with 40 s acquisition intervals for the resting parameters. These anomalies are due to integration effects which are related to the shape of the input fraction.

4.2. Photon integration

As mentioned in section 3.2, integration of the time–activity curve by the detector can introduce bias into the kinetic parameter estimates. The sampled version of the time–activity curve can vary depending on the duration of the acquisition interval and the time at which the acquisition interval begins relative to the starting point of the input function. This effect could be reduced by shifting the input function in time, in order to optimize the injection of tracer with respect to the detector acquisition interval.
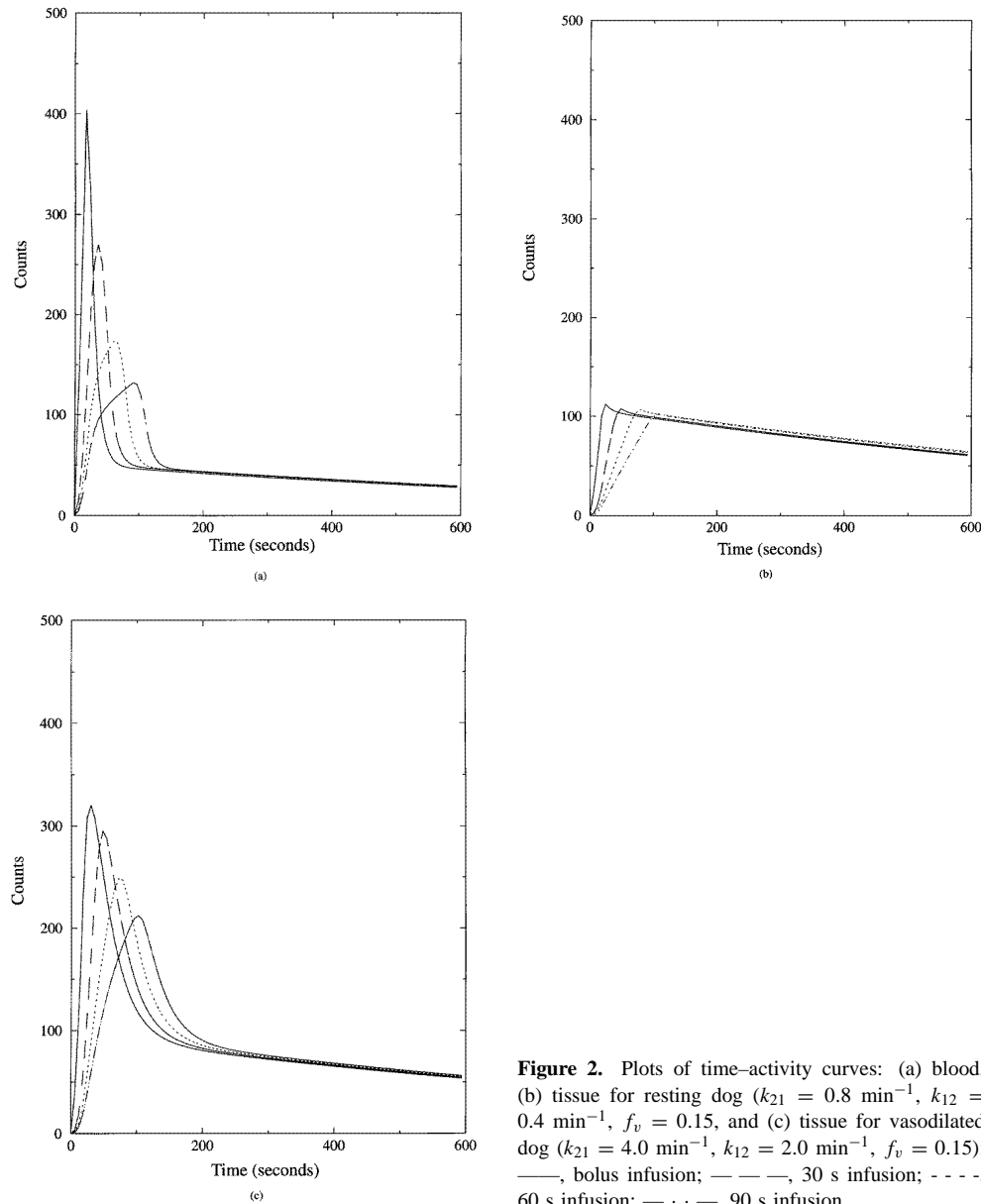
Figure 2. Plots of time–activity curves: (a) blood, (b) tissue for resting dog ($k_{21} = 0.8$ min^{-1}, $k_{12} = 0.4$ min^{-1}, $f_v = 0.15$, and (c) tissue for vasodilated dog ($k_{21} = 4.0$ min^{-1}, $k_{12} = 2.0$ min^{-1}, $f_v = 0.15$); ——, bolus infusion; — — —, 30 s infusion; - - - -, 60 s infusion; — · · —, 90 s infusion.

This is demonstrated by shifting the time–activity curves of figure 2(a) to optimize the parameter estimates. The time–activity curves are shifted by quarter intervals of that sampling interval, e.g., delay intervals of 0, 1.25, 2.5, and 3.75 s are used for 5 s acquisitions. Figure 5 shows results for estimates of k_{21} with the input function optimized for minimum bias. The optimization has little effect on bias for 5 and 10 s acquisitions because the time–activity curves are sufficiently sampled. However, the bias is significantly reduced for a 20 s acquisition with a bolus infusion and for a 40 s acquisition with a 30 s infusion. This occurs because the peak of the blood time–activity curve for the bolus infusion is at 20 s, while the peak for the 30 s infusion is at approximately 40 s. Thus, integration effects
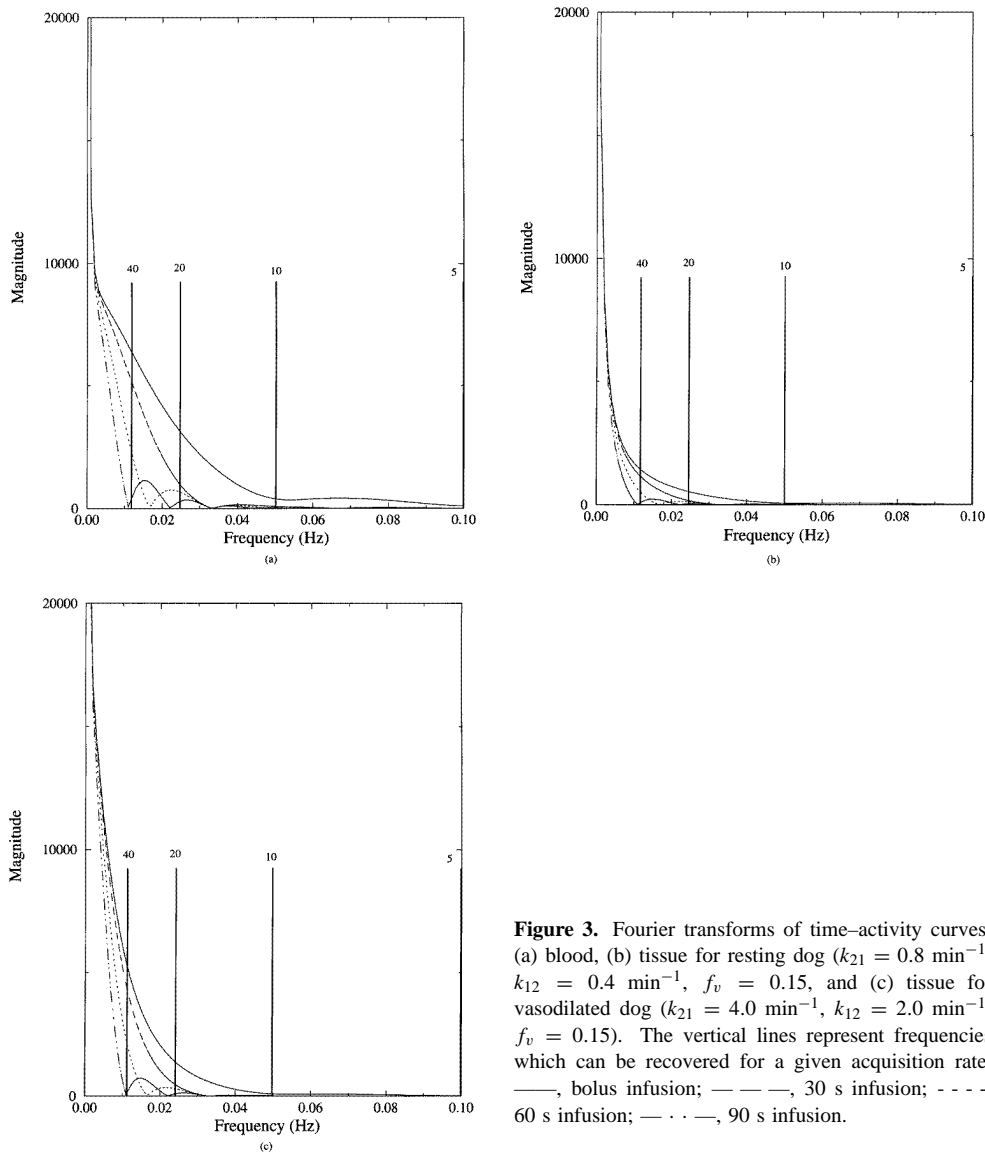
Figure 3. Fourier transforms of time–activity curves: (a) blood, (b) tissue for resting dog ($k_{21} = 0.8$ min^{-1}, $k_{12} = 0.4$ min^{-1}, $f_v = 0.15$, and (c) tissue for vasodilated dog ($k_{21} = 4.0$ min^{-1}, $k_{12} = 2.0$ min^{-1}, $f_v = 0.15$). The vertical lines represent frequencies which can be recovered for a given acquisition rate. ——, bolus infusion; — — —, 30 s infusion; - - - -, 60 s infusion; — · · —, 90 s infusion.

are greatest when the peak of the time–activity curve coincides with the integration period. This will depend on not only the injection time, but also the uptake time of the tracer, and would be difficult to control in practice. The most effective method of minimizing integration effects is to reduce the acquisition interval. The remaining results do not utilize any optimization.

4.3. Detector motion

The following results are obtained by modelling the three-detector rotating SPECT system which acquires 60 projection sets as it rotates over 360°. Also, a fixed detector SPECT system was modelled which acquires 60 projection sets with no rotation. The heart is
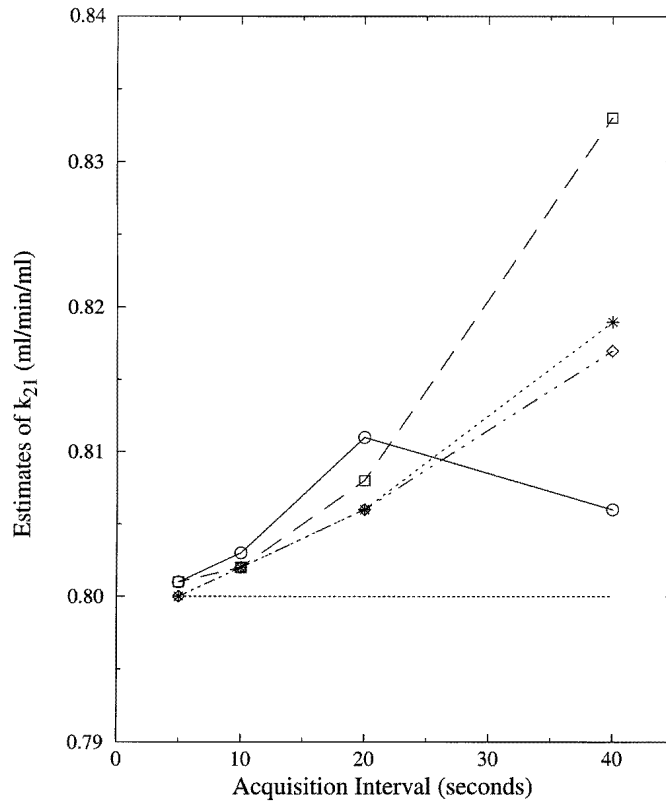
Figure 4. Estimates of k_{21} for resting kinetic parameters: $\bigcirc$, bolus infusion; $\square$, 30 s infusion; $\lozenge$, 60 s infusion; $*$, 90 s infusion; - - - -, actual value of k_{21}.

modelled with the MCAT phantom as described in section 3.3. Figure 6(a) shows estimates of washin against iteration number of the EM–ML algorithm for the fixed detector using a bolus infusion and 5, 10, 20, and 40 s acquisition intervals. The estimates obtained using the static detector system reach convergence at approximately 50 iterations. Results obtained with filtered backprojection are shown at iteration zero and compare well to those obtained with EM–ML as it asymptotically approaches convergence.

Figure 6(b) shows estimates of washin for the moving detector system using a bolus infusion. Unlike the static detector, estimates of washin do not converge as the iteration number is increased. The rate of divergence is least for a 5 s acquisition. Estimates obtained with filtered backprojection show relatively small levels of bias for all acquisition intervals. Figure 6(c) shows estimates of washin for the static detector system using a 90 s infusion. As with the bolus infusion, convergence is seen in the static detector after approximately 50 iterations. The increased bias in the 40 s acquisition most likely corresponds to integration effects and is present for both EM–ML and filtered backprojection. The results from the moving detector using a 90 s infusion are shown in figure 6(d). For 5, 10, and 20 s acquisition intervals, the divergence is not as rapid with the 90 s infusion as with the bolus infusion. However, estimates obtained with the 40 s acquisition interval diverge more rapidly with a 90 s infusion than with a bolus infusion. This estimate also had a large bias
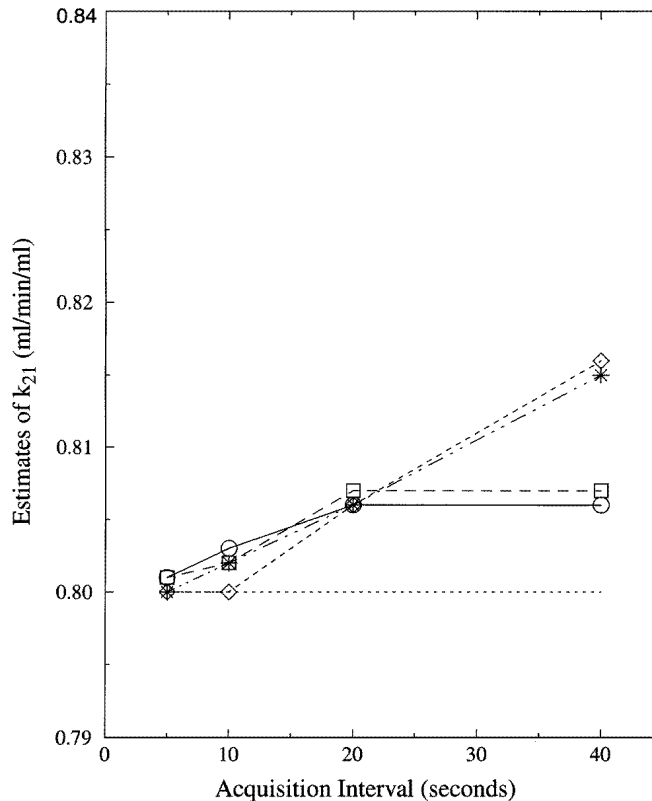
Figure 5. Estimates of k_{21} for resting kinetic parameters. The input function is shifted to obtain optimal estimates. ○, bolus infusion; □, 30 s infusion; ◇, 60 s infusion; *, 90 s infusion; - - - -, actual value of k_{21}.

when it was obtained using filtered backprojection. This bias is possibly introduced from integration effects as discussed in the previous section.

4.4. Photon statistics

Figure 7 shows results from estimates of washin with photon statistics included in the simulations to coincide with a 15 mCi injection of ^{99m}Tc-labelled teboroxime in a 35 kg dog. The mean and plus/minus one population standard deviation are shown for resting and vasodilated kinetics. One hundred realizations were performed. Noise in the projection data introduces variance in the estimates, which tends to dominate the bias from aliasing, detector motion, and integration. Variance and bias in the estimates is much greater for vasodilated rate constants than resting rate constants.

Figure 8 shows results with photon statistics corresponding to a 30 mCi injection of ^{99m}Tc-labelled teboroxime in a 35 kg dog. Increasing the simulated activity to correspond to a 30 mCi injection, rather than a 15 mCi injection, of ^{99m}Tc-labelled teboroxime reduces the variance of the kinetic parameter estimates. Variance reduction is greater than the factor of the square root of two that one might expect from a nonpropagating Poisson process.
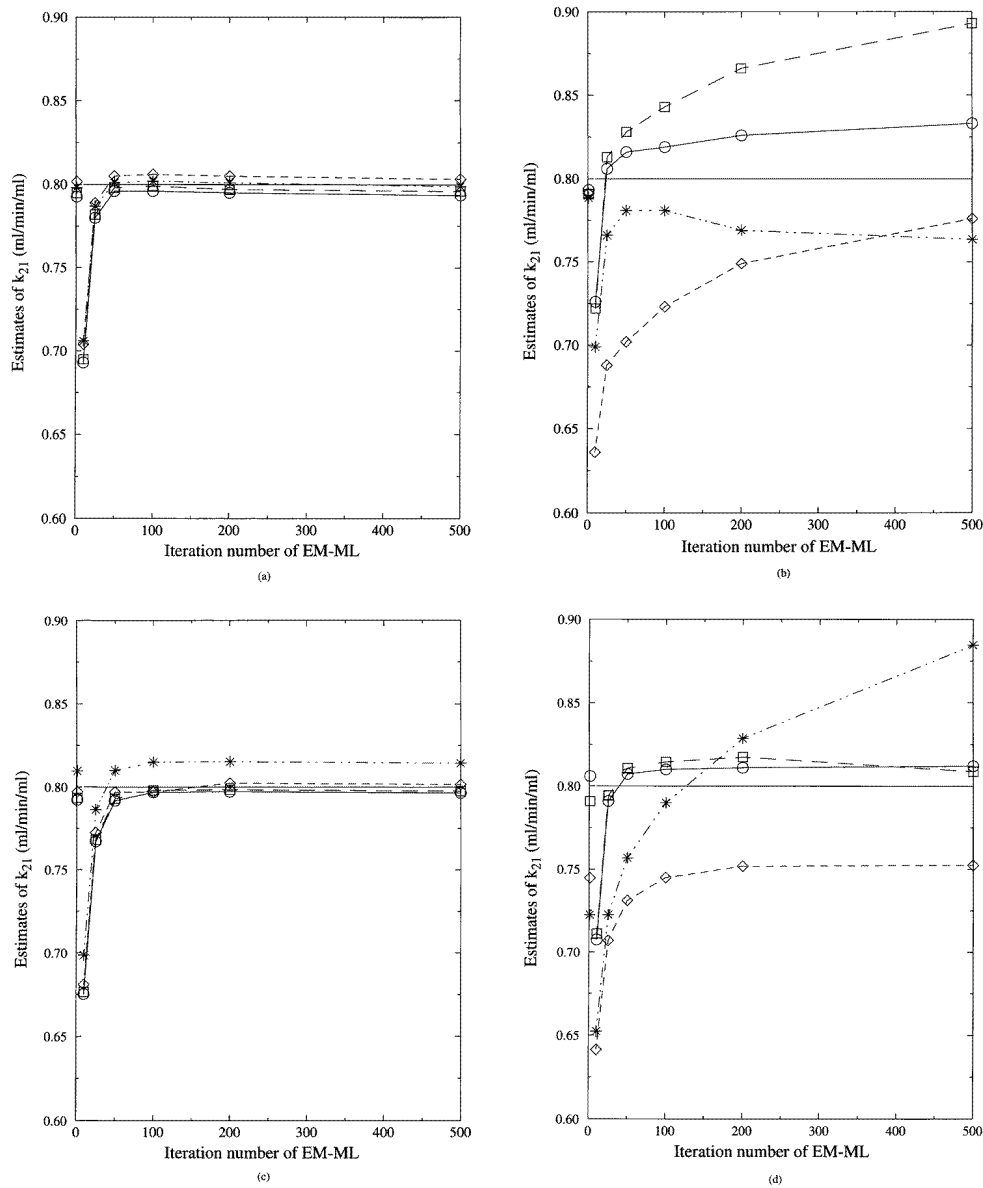
Figure 6. Estimates of k_{21} for varying iteration number of the EM–ML algorithm. Iteration zero corresponds to estimates obtained using filtered backprojection. (a) Fixed detector, bolus infusion; (b) moving detector, bolus infusion; (c) fixed detector, 90 s infusion; (d) moving detector, 90 s infusion. ○, 5 s infusion; □, 10 s infusion; ◇, 20 s infusion; ∗, 40 s infusion; - - - -, actual value of k_{21}.

Plots of absolute parameter bias against parameter variance are shown in figures 9–12. The plots show an absolute bias–variance curve for each acquisition interval. The results indicate that the optimal input function and acquisition interval is a function of both photon statistics and myocardial tissue kinetics.
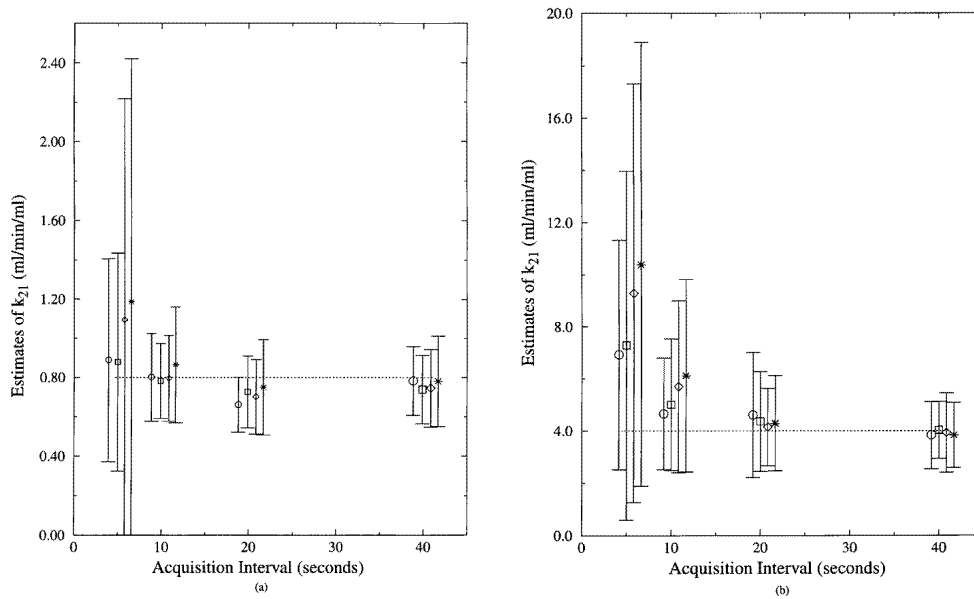
Figure 7. Estimates of k_{21} with noisy data generated to represent the counts in a 15 mCi injection of ^{99m}Tc-labelled teboroxime into a 35 kg dog. The symbol represents the mean from 100 realizations while the error bars represent plus/minus one standard deviation. (a) Resting kinetic parameters; (b) vasodilated kinetic parameters. $\bigcirc$, bolus infusion; $\square$, 30 s infusion; $\Diamond$, 60 s infusion; $*$, 90 s infusion; - - - -, actual value of k_{21}.

The plot of figure 9 corresponds to resting kinetic parameters with noise simulating a 15 mCi injection of ^{99m}Tc-labelled teboroxime in a 35 kg dog. The largest variance occurs for a 5 s acquisition interval. The variance is reduced by using a sharper input function. Variance levels decrease when 10, 20, and 30 s acquisition intervals are used. The least bias is observed with a 10s acquisition and a bolus infusion. The most bias (ignoring 5 s acquisitions) is observed with a 20 s acquisition and a bolus infusion. This is most likely attributed to integration effects, which are also observed when a 40 s acquisition interval is used with 30 and 60 s infusions.

The results of figure 10 correspond to vasodilated kinetic parameters with noise simulating a 15 mCi injection of ^{99m}Tc-labelled teboroxime into a 35 kg dog. Variance levels are much larger than observed for resting kinetics. The variance consistently decreases as the acquisition interval is lengthened. Along with variance levels, bias is also decreased as the acquisition interval is lengthened. This suggests that when kinetics are increased, count levels become more critical than with resting kinetics. The reduction in aliasing and subsequently in bias which is produced with a 5 s acquisition is not noticeable because of the large levels of variance. Bias and variance are less sensitive to input function shape than acquisition interval. For 5 and 10 s acquisitions, the least bias and variance was observed with shorter infusion rates. This trend was reversed with 20 s acquisitions. Forty second acquisitions had the least bias when 30 and 60 s infusions were used. In general as the acquisition interval was increased and subsequently count levels were increased, the input function shape had a less noticeable effect.

The results of figure 11 correspond to resting kinetic parameters with nose simulating a 30 mCi injection of ^{99m}Tc-labelled teboroxime into a 35 kg dog. Note that the higher
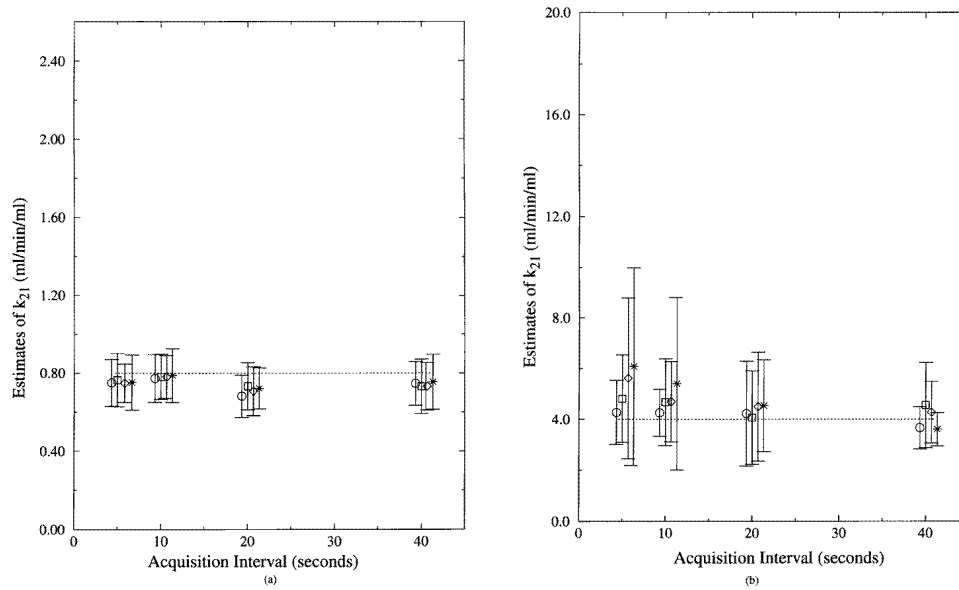
Figure 8. Estimates of k_{21} with noisy data generated to represent the counts in a 30 mCi injection of ^{99m}Tc-labelled teboroxime into a 35 kg dog. The symbols represent the means from 100 realizations while the error bars represent plus/minus one standard deviation. (a) Resting kinetic parameters; (b) vasodilated kinetic parameters. $\bigcirc$, bolus infusion; $\square$, 30 s infusion; $\lozenge$, 60 s infusion; $*$, 90 s infusion; - - - -, actual value of k_{21}.

photon count rates result in much smaller levels of variance than were observed for resting parameters in figure 9. The bias is also much lower with better photon statistics, with variance levels approximately an order of magnitude smaller than the bias levels. The results show that effects from varying the acquisition interval are much less distinct when count levels are increased. The minimum levels of variance are now observed with a 5 s acquisition and a 60 s infusion, although the differences in variance are not large for any of the estimates. The plots show no distinct trends, with the least bias arising with a 10 s acquisition and a bolus infusion.

The results of figure 12 correspond to vasodilated kinetic parameters with noise simulating a 30 mCi injection of ^{99m}Tc-labelled teboroxime into a 35 kg dog. Note that variance levels are now more sensitive to acquisition interval than with the resting parameters. Five second acquisitions now give large levels of variance when 60 and 90 s infusion rates are used. However, the variance levels are significantly lower than those observed when the injection was only 15 mCi. Levels of variance for 10 s acquisition are not as sensitive to input function shape as for a 5 s acquisition, although there is a slight reduction in variance when a bolus infusion is used. Bias is reduced significantly by using a sharper input function for both 5 and 10 s acquisitions. Figures 9–12 suggest that the acquisition interval is in general more critical than the infusion length, particularly when photon statistics are low.

Table 1 summarizes the optimal estimates obtained with each simulated protocol. The results imply that the input function shape and acquisition interval must be selected carefully depending on the count levels and kinetics associated with the protocol. However, a careful analysis of the results shown in figures 9–12 show that in some cases there is very little difference in kinetic parameter estimates for different input function shapes and
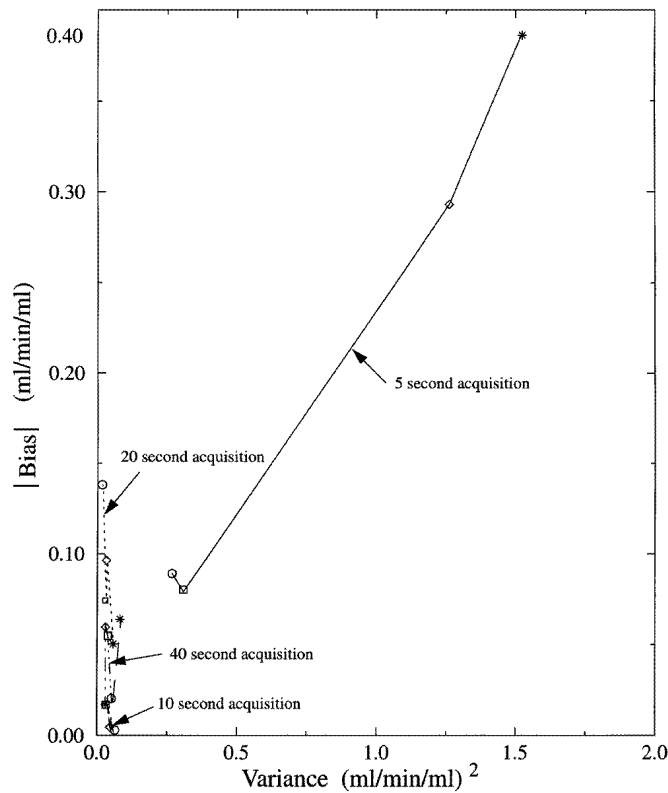
Figure 9. Absolute bias against variance for resting kinetic parameter estimates with noise simulating a 15 mCi injection of ^{99m}Tc-labelled teboroxime into a 35 kg dog: $\bigcirc$, bolus infusion; $\square$, 30 s infusion; $\diamond$, 60 s infusion; $*$, 90 s infusion.

image acquisition intervals. When resting kinetics are assumed with a 15 mCi injection of ^{99m}Tc-labelled teboroxime into a 35 kg dog, a bolus infusion always provided the optimal estimates of kinetic parameters. The least bias was observed with a 10 s acquisition, the least variance with a 20 s acquisition, and the estimates with the least total $\sqrt{\text{bias}^2 + \text{variance}}$ were obtained with a 10 s acquisition. Longer acquisition intervals result in the most accurate estimates of kinetic parameters when vasodilated kinetics are assumed. When the count rates were doubled, longer infusions and shorter acquisitions provided more accurate estimates of kinetic parameters when resting kinetics were simulated. When kinetics are increased to simulate vasodilated parameters, longer acquisitions result in more optimal estimates. This indicates that better signal-to-noise ratios are required when fast kinetics are to be estimated.

5. Discussion

This study investigated the effect of input function shape and image acquisition interval on estimates of washin for dynamic cardiac SPECT. Analogous studies have been carried out in dynamic PET (Cunningham and Jones 1993, Raylman *et al* 1993, Herrero *et al* 1989, Mazoyer *et al* 1986); however, count levels in dynamic cardiac SPECT are much poorer than
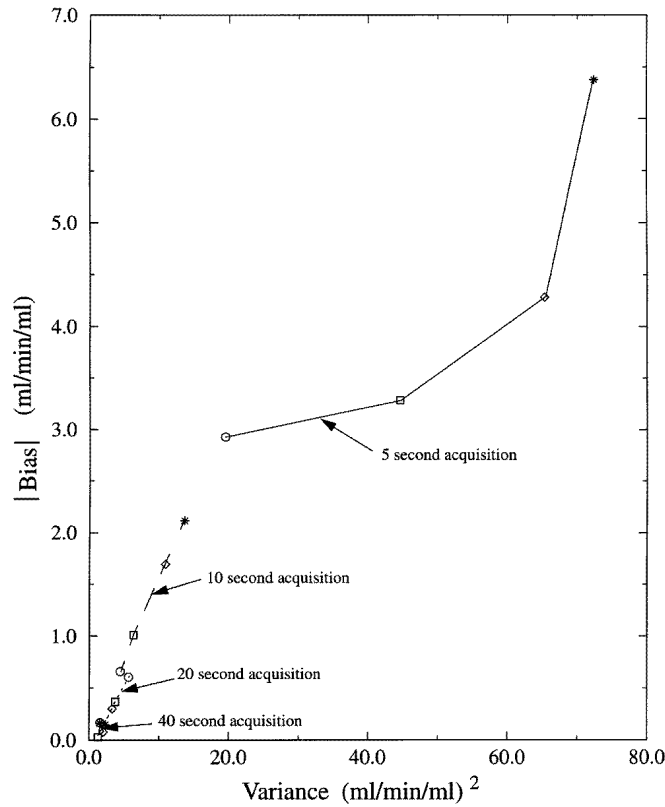
Figure 10. Absolute bias against variance for vasodilated kinetic parameter estimates with noise simulating a 15 mCi injection of ^{99m}Tc-labelled teboroxime into a 35 kg dog: $\bigcirc$, bolus infusion; $\square$, 30 s infusion; $\Diamond$, 60 s infusion; $*$, 90 s infusion.

Table 1. A summary of results from simulations with photon noise (100 realizations). Changes in estimates of washin for different input function shape and image acquisition interval are not always significant. Figures 7–12 should be addressed to best interpret the data.

Protocol	15 mCi resting	15 mCi vasodilated	30 mCi resting	30 mCi vasodilated
Minimum bias	bolus infusion 10 s acq	30 s infusion 40 s acq	30 s infusion 10 s acq	30 s infusion 20 s acq
Minimum variance	bolus infusion 20 s acq	30 s infusion 40 s acq	60 s infusion 5 s acq	90 s infusion 40 s acq
Minimum $\sqrt{\text{bias}^2 + \text{variance}}$	bolus infusion 10 s acq	30 s infusion 40 s acq	30 s infusion 10 s acq	90 s infusion 40 s acq

those in dynamic cardiac PET studies. This causes variance levels in estimates of washin to be much larger than in dynamic cardiac PET studies. This variance can be reduced by increasing the dose, applying a faster input function, or increasing the acquisition interval. This study showed that the choice of acquisition interval and input function shape depends on both the count levels and the tissue kinetics. Although bias is present in the estimates of washin, variance levels tend to dominate any effect from bias. When variance levels
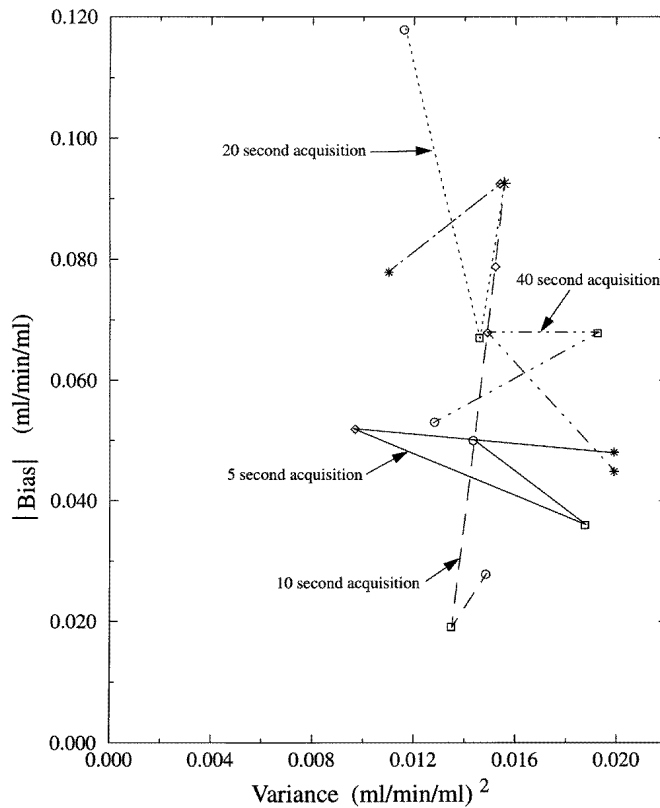
Figure 11. Absolute bias against variance for resting kinetic parameter estimates with noise simulating a 30 mCi injection of ^{99m}Tc-labelled teboroxime into a 35 kg dog: O, bolus infusion; □, 30 s infusion; ◇, 60 s infusion; ∗, 90 s infusion.

are high, the most effective method of reducing this variance is to use a longer acquisition interval, and thus increase counts. When count levels are low, a sharp input function also reduces variance levels. When simulated count levels are doubled, variance levels can be greatly reduced. At these count levels, the acquisition interval does not have as significant an effect on variance levels as observed with lower count levels, and shorter acquisition intervals can be used to reduce aliasing.

Bias is introduced in estimates of washin through aliasing of the time–activity curves. This bias can be reduced by acquiring dynamic images more rapidly, thus recovering more of the temporal changes in the time–activity curves. Bias can also be reduced by spreading the infusion of the radioactive tracer over time. This reduces the high frequencies in the tracer, resulting in less aliasing and consequently less bias. This also has the advantage of allowing longer acquisition intervals to be used, resulting in less data storage. However, the input function must be sufficiently sharp that the system kinetics can be adequately tracked.

The relative starting time position of the time–activity curve with respect to the integration interval of the detector can also introduce bias into estimates of washin. This effect can be reduced by shifting the input function so that it is optimized with respect to the acquisition interval. However, this optimization is impractical because the rate of uptake will vary with patient and this rate will have a direct effect on bias caused by integration.
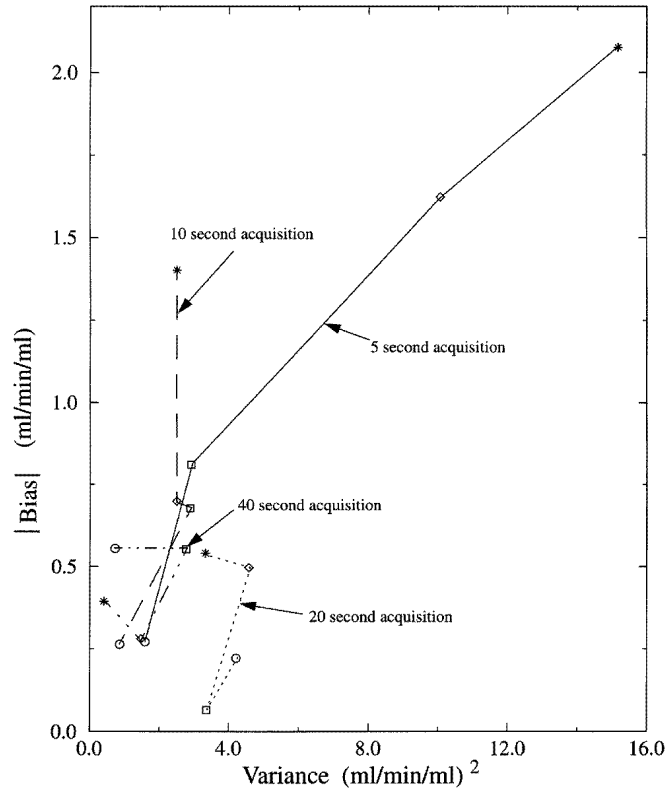
Figure 12. Absolute bias against variance for vasodilated kinetic parameter estimates with noise simulating a 30 mCi injection of ^{99m}Tc-labelled teboroxime into a 35 kg dog: $\bigcirc$, bolus infusion; $\square$, 30 s infusion; $\lozenge$, 60 s infusion; $*$, 90 s infusion.

The best methods of reducing effects due to integration are to increase the infusion length and reduce the image acquisition interval.

Another cause of bias is the detector motion necessary in the three-detector dynamic SPECT system. Rotation of the detector heads introduces bias by producing inconsistent projection data. When dynamic images are reconstructed with the EM–ML algorithm, kinetic parameter estimates based on these images do not converge as the iteration number of the algorithm increases. Thus divergence of the estimates with iteration of EM–ML depends on both the shape of the input function and the acquisition interval, although the effect is less severe when shorter acquisition intervals are used. It has been shown that bias can potentially be reduced by estimating the kinetic parameters directly from the projections (Zeng *et al* 1995).

The aforementioned effects introduce bias into the estimates; however, for typical dynamic SPECT count levels, variance in the kinetic parameter estimates tends to overwhelm bias caused by these physical effects. Additionally, as shown by Welch *et al* (1995) and in this study, bias in estimates of washin is also increased when photon counts are reduced to levels observed for a 15 mCi injection of ^{99m}Tc-labelled teboroxime. Variance and bias in estimates were shown to be quite large for low count rates; however, both can be reduced significantly by modest increases in photon statistics. In this study, doubling the counts resulted in a reduction in variance greater than the expected factor of the square root of

two. Both the reduction in bias and the greater-than-expected reduction in variance are possibly attributable to the skewed Poisson distribution (Welch *et al* 1995), although more work is necessary to clearly understand this. When count rates cannot be increased by using a larger dose, variance can be reduced significantly by lengthening the acquisition interval. Additional reductions in variance are obtained by using a sharper input function.

The results in this study compare well with results in the PET literature when 30 mCi injections of ^{99m}Tc-labelled teboroxime were simulated with resting kinetics. For instance, in a study described by Raylman *et al* (1993), 30 s infusions were found to result in the optimum estimates of kinetic parameters when 5 and 10 s acquisitions were employed. Also, in a study by Mazoyer *et al* (1986), it was found that the precision in the estimates of kinetic parameters did not change greatly when the acquisition interval was reduced below 30 s regardless of input function shape. As the counts were reduced and kinetics increased, however, longer acquisition intervals were required to obtain optimum estimates of washin. This suggests that optimum protocols for dynamic cardiac PET are not directly transferable to dynamic cardiac SPECT.

Variance of the washin estimates is affected by the kinetics of the myocardial tissue. As the kinetics are increased, variance levels in the estimates are also increased. This variance can be reduced by increasing the acquisition interval and thus increasing photon counts. Although increasing the acquisition interval would be expected to increase bias in the estimates due to undersampling, this increase in bias is insignificant compared to the gains from improved signal-to-noise ratios. More work is necessary to understand the effects of increased kinetic values on estimates of these kinetic parameters. This effect could possibly be related to the ill conditioning of the transfer function matrix of the governing equation. When washout, k_{12}, is increased, the condition number of the transfer function matrix increases because of the exponential kernel. This effect could possibly be reduced through regularization in the fitting procedure. This ill conditioning is closely tied to the signal-to-noise ratio of the system, as it is significantly reduced when counting statistics are improved.

There are also other factors which affect bias through input function shape and image acquisition interval which were not directly addressed in this study. Welch *et al* (1995) demonstrated the importance of ROI location to bias and variance of parameters. The location of the ROI could also affect the necessary temporal resolution and peak dynamic projection set counts, which would in turn be affected by input function shape and image acquisition interval. The use of rotated short axis slices when drawing ROIs will also affect estimates, primarily by smoothing the data, thus increasing bias and reducing variance. Because both bias and precision appear to be directly related to signal-to-noise ratios, another issue to be addressed is the count levels associated with dynamic cardiac SPECT studies with human patients. In addition, methods for regularizing the ill posedness associated with faster kinetic rate constants should also be an area of investigation. More work must also be done to understand the effects on kinetic parameter estimates of iteration number in the EM–ML algorithm, attenuation, geometric point response, scatter, and angular sampling.

References

Barrett H H, Wilson D W and Tsui B M W 1994 Noise properties of the EM algorithm: I. Theory *Phys. Med. Biol.* **39** 833–46

Bergmann S R, Herrero P, Markham J, Weinheimer C J and Walsh M N 1989 Noninvasive quantitation of myocardial blood flow in human subjects with oxygen-15-labeled water and positron emission tomography *J. Am. Coll. Cardiol.* **14** 639–52

Coxson P G, Salmeron E M, Huesman R H and Mazoyer B M 1992 Simulation of compartmental methods for kinetic data from a positron emission tomograph *Comput. Methods Prog. Biomed.* **37** 205–14

Cunningham V J and Jones T 1993 Spectral analysis of dynamic PET studies *J. Cereb. Blood Flow Metab.* **13** 15–23

Gullberg G T, Huesman R H, Malko J A, Pelc N J and Budinger T F 1985 An attenuated projector–backprojector for iterative SPECT reconstruction *Phys. Med. Biol.* **30** 799–816

Gullberg G T, Huesman R H, Ross S G, Di Bella E V R, Zeng G L, Reutter B W, Christian P E and Foresti S A 1997 Dynamic cardiac single photon emission computer tomography *Nuclear Cardiology: State of the Art and Future Directions* ed B L Zaret and G A Beller (New York: Mosby–Year Book) at press

Herrero P, Markham J and Bergmann S R 1989 Quantitation of myocardial blood flow with $H_2{}^{15}O$ and positron emission tomography: assessment and error analysis of a mathematical approach *J. Comput. Assist. Tomogr.* **13** 862–73

Herrero P, Markham J, Shelton M E and Bergmann S R 1992 Implementation and evaluation of a two-compartment model for quantification of myocardial perfusion with rubidium-82 and positron emission tomography *Circ. Res.* **70** 496–507

Huesman R H, Gullberg G T, Greenberg W L and Budinger T F 1977 *Users' Manual—Donner Algorithms for Reconstruction Tomography* LBL-5604

Huesman R H, Knittel B L, Mazoyer B M, Coxson P G, Salmeron E M, Klein G J, Reutter B W and Budinger T F 1995 Notes on RFIT: A program for fitting compartment models to region-of-interest dynamic emission tomography data LBL-37621 *version 4.3*

Huesman R H and Mazoyer B M 1987 Kinetic data analysis with a noisy input function *Phys. Med. Biol.* **32** 1569–79

Lange K and Carson R 1984 EM reconstruction algorithms for emission and transmission tomography *J. Comput. Assist. Tomogr.* **8** 306–16

Mazoyer B M, Huesman R H, Budinger T F and Knittel B L 1986 Dynamic PET data analysis *J. Comput. Assist. Tomogr.* **10** 645–53

Mullani N A, Goldstein R A, Gould K L, Marani S K, Fisher D J, O'Brien H A Jr and Loberg M D 1983 Myocardial perfusion with rubidium-82. I. Measurements of extraction fraction and flow with external detectors *J. Nucl. Med.* **24** 898–906

Muzik O, Beanlands R S B, Hutchins G D, Manger T J, Nguyen N and Schwaiger M 1993 Validation of nitrogen-13-ammonia tracer kinetic model for quantification of myocardial blood flow using PET *J. Nucl. Med.* **34** 83–91

Raylman R R, Caraher J M and Hutchins G D 1993 Sampling requirements for dynamic cardiac PET studies using image-derived input functions *J. Nucl. Med.* **34** 440–7

Shepp L A and Vardi Y 1982 Maximum likelihood reconstruction for emission tomography *IEEE Trans. Med. Imaging* **1** 113–22

Smith A M and Gullberg G T 1994 Dynamic cardiac SPECT computer simulations for teboroxime kinetics *IEEE Trans. Nucl. Sci.* **41** 1626–33

Smith A M, Gullberg G T and Christian P E 1996 Experimental verification of technetium 99m-labeled teboroxime kinetic parameters in the myocardium with dynamic single-photon emission computed tomography: reproducibility, correlation to flow, and susceptibility to extravascular contamination *J. Nucl. Cardiol.* **3** 130–42

Smith A M, Gullberg G T, Christian P E and Datz F L 1994 Kinetic modeling of teboroxime using dynamic SPECT imaging of a canine model *J. Nucl. Med.* **35** 484–95

Stewart R E, Schwaiger M, Hutchins G D, Chiao P C, Gallagher K P, Nguyen N, Petry N A and Rogers L 1990 Myocardial clearance kinetics of technetium-99m SQ30217: a marker of regional myocardial blood flow *J. Nucl. Med.* **31** 1183–90

Terry J A, Tsui B M W, Perry J R, Hendricks J L and Gullberg G T 1990 The design of a mathematic phantom of the upper human torso for use in 3-D SPECT imaging research *Biomedical Engineering: Opening New Doors* ed D C Mikulecky and A M Clarke (New York: University Press) pp 185–90

Tsui B M W, Zhao X D, Gregoriou G K, Lalush D S, Frey E C, Johnson R E and McCartney W H 1994 Quantitative cardiac SPECT reconstruction with reduced image degradation due to patient anatomy *IEEE Trans. Nucl. Sci.* **41** 2838–44

Welch A, Smith A M and Gullberg G T 1995 An investigation of the effect of finite system resolution and photon noise on the bias and precision of dynamic cardiac SPECT parameters *Med. Phys.* **22** 1829–36

Wilson D W and Tsui B M W 1993 Noise properties of filtered-backprojection and ML–EM reconstructed emission tomographic images *IEEE Trans. Nucl. Sci.* **40** 1198–203

Wilson D W, Tsui B M W and Barrett H H 1994 Noise properties of the EM algorithm: II. Monte Carlo simulations *Phys. Med. Biol.* **39** 847–71

Zeng G L and Gullberg G T 1992 Frequency domain implementation of the three-dimensional geometric point response correction in SPECT imaging *IEEE Trans. Nucl. Sci.* **39** 1444–53

Zeng G L, Gullberg G T and Huesman R H 1995 Using linear time-invariant system theory to estimate kinetic parameters directly from projection measurements *IEEE Trans. Nucl. Sci.* **42** 2339–46

Zeng G L, Gullberg G T, Tsui B M W and Terry J A 1991 Three-dimensional iterative reconstruction algorithms with attenuation and geometric point response correction *IEEE Trans. Nucl. Sci.* **38** 693–702